Graphene Structures at an Extreme Degree of Buckling

Youdong Mao,*,† Wei L. Wang,‡,∥ Dongguang Wei,§,∥ Efthimios Kaxiras,‡ and Joseph G. Sodroski*,†,⊥

†Dana-Farber Cancer Institute, Department of Pathology, Harvard Medical School, Boston, Massachusetts 02115, United States, ‡Department of Physics, School of Engineering and Applied Sciences, Harvard University, Cambridge, Massachusetts 02138, United States, §Carl Zeiss NTS, LLC, One Corporation Way, Peabody, Massachusetts 01960, United States, and ⊥Department of Immunology and Infectious Disease, Harvard School of Public Health, Boston, Massachusetts 02115, United States. ∥These authors contributed equally to this work.

ABSTRACT The distinctive properties of graphene sheets may be significantly influenced by the presence of corrugation structures. Our understanding of these graphene structures has been limited to the mesoscopic scale. Here we characterize angstrom-scale periodic buckling structures in free-standing graphene bilayers produced by liquid-phase processing in the absence of specific substrates. Monochromated, aberration-corrected transmission electron microscopy with sub-angstrom resolution revealed that the unit structures in the major buckling direction consist of only two and three unit cells of graphene's honeycomb lattice, resulting in buckling wavelengths of 3.6 ± 0.5 and 6.4 ± 0.8 Å, respectively. The buckling shows a strong preference of chiral direction and spontaneously chooses the orientation of the lowest deformation energy, governed by simple geometry rules agreeing with Euler buckling theory. Unexpectedly, the overall buckled structures demonstrate geometric complexity with cascaded features. First-principles calculations suggest that significant anisotropic changes in the electronic structure of graphene are induced by the buckling.

KEYWORDS: graphene · aberration-corrected transmission electron microscopy · Euler buckling instability · electronic structure · density functional theory

Graphene, a two-dimensional (2D) carbon crystal, has elicited widespread scientific interest.[1−5] The physical properties of graphene may be significantly influenced by the presence of corrugations.[6−15] Periodic ripples represent an especially desirable means to tailor graphene's properties owing to their controllability.[15−18] The formation of all known periodic ripples, whose wavelengths range from 2 nm to 5 μm, is highly dependent on the use of specific substrates.[16−19] It is unknown whether graphene can endure an extreme degree of buckling on the angstrom scale and how graphene reorganizes its structure in response to conditions that promote such buckling in the absence of specific substrates. Experimental and theoretical studies of these problems would provide insight into the general properties of 2D atomic crystals.

The direct, unambiguous observation of an angstrom-scale buckling structure in graphene is challenging, because the in-plane compression of the graphene lattice and the out-of-plane displacement of carbon atoms may cause the atomic details to be hidden behind the information limit of conventional electron microscopic instruments. Recent advances in aberration-corrected transmission electron microscopy (TEM) have improved its resolution limit to the sub-angstrom level.[22] We employed a monochromated, aberration-corrected TEM with a field-emission gun, Libra 200MC, operating at 80 kV, to conduct this study. The electron monochromator and the objective lens spherical aberration corrector modified the envelope function and the contrast transfer function relative to those of conventional field-emission TEM, resulting in a narrower depth of field at the focal plane of image formation and directly interpretable atomic images.[22] In a typical bright-field TEM image of a flat graphene area, the Fourier spectrum of the image demonstrated that the in-plane information limit of this microscope was well adjusted down to 0.58 Å in this study (Supporting Information, Figure S1).

RESULTS AND DISCUSSION

The graphene was prepared by liquid-phase exfoliation of graphite in organic solvent, *N*-methyl-pyrrolidone (NMP).[20] The graphene dispersion was deposited onto a holey carbon grid and vacuum dried before loading into the electron microscope specimen chamber (see Methods). Only the graphene sheets suspended in the empty holes of the carbon grid were subjected to TEM analysis. A previous study found that the graphene sheets prepared in NMP by this method are free of oxidation and defects, that about 70% of them have no more than three layers and that about 28% are monolayers.[20] Our results were consistent with these findings.

In one layer of a free-standing graphene bilayer, we observed a one-dimensional (1D) periodic buckling structure with a

*Address correspondence to youdong_mao@dfci.harvard.edu, joseph_sodroski@dfci.harvard.edu.

Received for review November 20, 2010 and accepted December 24, 2010.

Published online January 11, 2011
10.1021/nn103153x

© 2011 American Chemical Society

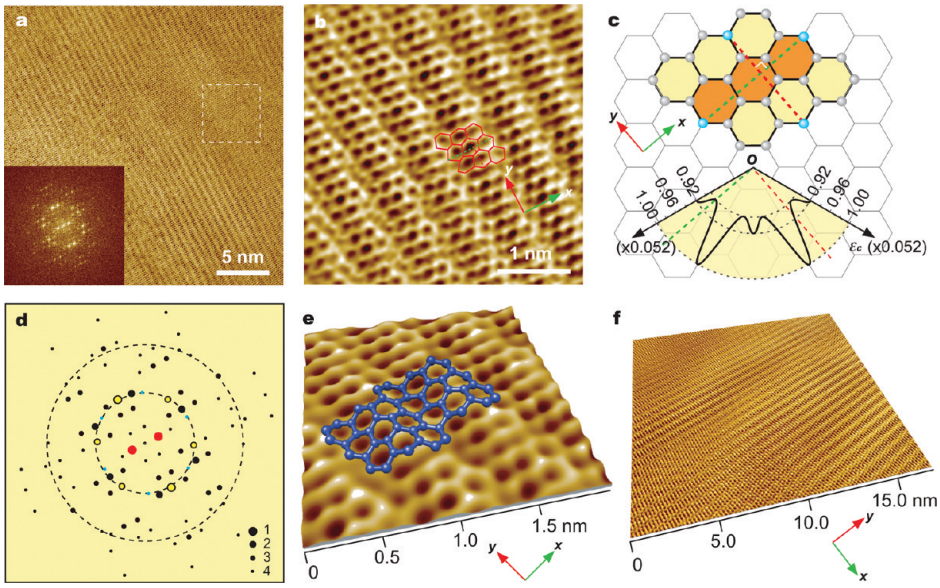

Figure 1. The 6.4 Å periodic buckling structure in a free-standing graphene bilayer. (a) TEM image of the buckling structure in one layer of a graphene bilayer. Inset, the Fourier spectrum of the image. The area bounded by the dashed box lacks buckling amplitude and coincides with a mesoscopic ripple. (b) Sub-angstrom resolution TEM reveals details of the reorganized carbon atoms and graphene lattices in the buckled region. The unit buckling manifold is marked by red hexagons. (c) The intrinsic geometric rule in the unit buckling manifold (upper panel) and the calculated angular distribution of nominal critical strain (ε_c) at a distance of three unit cells (lower panel, drawn in polar coordinate system) that guides the buckling orientation and wavelength selection. The green dashed line parallels the buckling direction. The red dashed line is orthogonal to the green dashed line. Only $2\pi/3$ angular range is shown for the angular distribution of ε_c due to its 6-fold symmetry. (d) The merged Fourier spectrum of the 6.4 Å buckling structure. The image quality (IQ) value,[29] from 1 to 4, is shown as the spot size from large to small. The red spots indicate the major buckling wavelength at 6.4 Å. The yellow spots indicate the major diffractions arising from the original graphene lattices. The blue spots indicate the reflections from the other nonbuckled layer of the graphene bilayer, which has about a $\pi/6$ rotation relative to the buckled layer. (e) The 3D reconstruction of the topographic view of the periodic buckling structure. The DFT-calculated 3D atomic configuration of the buckling structure with the lowest deformation energy (0.24 eV/atom) at the observed strain (0.09 in the *x*-direction), shown as a blue ball−stick model, was fitted into the 3D map. The buckling amplitude in the *x*-direction was determined to be ~1.2 Å; no obvious amplitude is observed in the *y*-direction. (f) The 3D perspective view of the buckling structure reconstructed from a TEM image demonstrates that the 6.4 Å buckling structure is nested within the mesoscopic ripples. In (b−f), the green arrows indicate the buckling orientation (*x*-direction), and the red arrows indicate the orthogonal *y*-direction.

wavelength of 6.4 ± 0.8 Å that is approximately composed of three consecutive unit cells of the hexagonal lattice, as shown in Figure 1. A sub-angstrom resolution TEM image (Figure 1b) shows that the periodic behavior of the buckling is strongly suppressed in the dimension orthogonal to the buckling orientation. The minimum unit of the buckling manifold may be approximately modeled by a 3 × 3 array of graphene's unit cells, whose three-dimensional (3D) structure lacks symmetry (Figure 1e). Only mesoscopic, randomly distributed ripples and no angstrom-scale buckling behaviors were observed in the other layer of the graphene bilayer.

Another buckling structure with a wavelength of 3.6 ± 0.5 Å was found in a folded graphene monolayer in the vicinity of the folding edge (Figure 2). The unit manifold in the major buckling direction comprises only two hexagonal unit cells (Figure 3a and b). This represents an extreme case for a buckled graphene layer, because a buckling wavelength comprising just one unit cell would generate at least 10 times higher deformation energy than that generated by the currently observed atomic conformation [24,25] and thus is energetically prohibited. Figure 3a clearly shows that the seemingly 1D buckling texture is actually decorated in detail by a highly ordered 2D array of unit buckling manifolds, each of which is composed of a 2 × 3 array of unit cells (Figure 3b). The 3D structure of the unit buckling manifold (Figure 3d) demonstrates twofold centrosymmetry (*P*2). Because the buckling in the *x*-direction markedly increases the bending rigidity in the *y*-direction,[24,25] a 2 × 3 array of unit cells might be the smallest unit configuration for spontaneous periodic buckling in graphene. The TEM images of the buckling structures (Figures 1−3) are not consistent with moiré fringe patterns of graphene bilayers (Supporting Information, note S1 and Figure S2).

Crystallographic analyses of the angstrom-scale buckling structures suggest common rules for the selection of buckling orientation and wavelength that are intrinsic to the geometry of the graphene lattice. In the 6.4 Å buckling structure, the buckling direction parallels the line intersecting the two most distant carbon atoms with *P*2 symmetry in three consecutive hexagonal cells, as illustrated in Figure 1c. A similar rule governs the 3.6 Å buckling structure, where the two

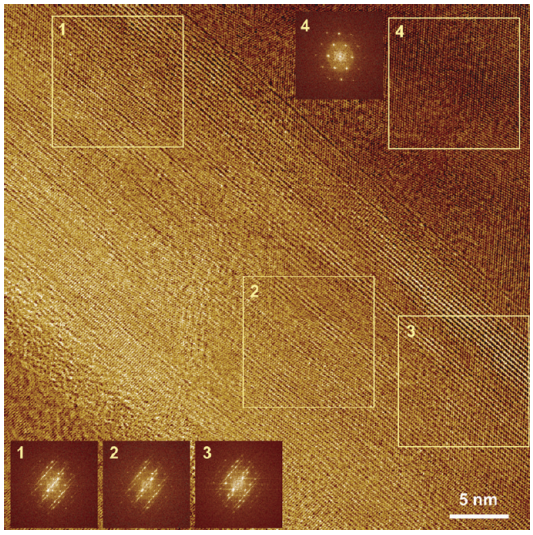

Figure 2. Aberration-corrected high-resolution TEM image of 3.6 Å periodic buckling in a folded graphene monolayer. Four image areas, boxed by yellow lines and numbered, are associated with the correspondingly numbered Fourier spectra in the insets. Comparison of Fourier spectra 1−3 suggests that they share a common major structure, though they have slight changes in minor features indicated by the diffraction spots beyond 1.0 Å. The major buckling direction orients strictly perpendicular to the folding line. Box 4 shows the background planar graphene sheet, providing an *in situ* control for crystallographic analysis.

most distant carbon atoms with *P*2 symmetry in two neighboring hexagonal cells define the major buckling orientation (Figure 3b). These geometry rules directly link the selection of buckling orientation to the wavelength. Furthermore, the folding direction in the 3.6 Å buckling structure is precisely orthogonal to the major buckling orientation (Figures 2 and 3b). The 3.6 Å buckling structure extends to the folding edge that defines the boundary condition of the overall buckling manifold; this observation suggests that the buckling and folding behaviors are highly coupled under the same geometry rules.

According to the classic theory of the Euler buckling instability, the critical strain (ε_c) of compression gives rise to the onset of buckling.[23,24] Below ε_c, there is only in-plane deformation for the graphene lattice. To understand the energetic basis of the observed geometry rules, we calculated ε_c at a distance of two or three unit cells as a function of the chiral direction (see Supporting Information, note S2 for details). The results, shown in lower panels in Figures 1c and 3b, reveal that the buckling orientations in the 6.4 and 3.6 Å buckling structures correspond to the smallest ε_c in its angular distribution at the distance of three and two unit cells, respectively. Thus, the buckling spontaneously chooses the direction of the lowest buckling energy matching its wavelength. To ascertain this result, we performed first-principles calculations of the buckling structures using the density functional theory (DFT) (see Methods). The *ab initio* graphene structures of the lowest deformation energy under compression buckle exactly along the experimentally observed directions; the entire atomic configurations closely match the 3D buckling structures reconstructed from the *Z* contrast of the TEM micrographs (Figures 1e and 3d). The consistency between experimental observations, *ab initio* calculations and Euler buckling theory, implies that the geometry rules are intrinsic properties of graphene's buckling at this fine level and are independent of specific interactions between graphene and other materials (like solvents or TEM grids). This contrasts with the mesoscopic periodic ripples,[16−19] where no similar intrinsic geometry rules were observed. Rather, their behaviors are highly dependent on the specific interaction between graphene and substrate and are governed by the mesoscopic elasticity of graphene sheets,[16,24−27] where the geometric details of the graphene lattice work in a mean-field manner.

More intriguingly, the overall buckling manifolds demonstrate geometric complexity with cascaded features. The 6.4 Å buckling structure was seen to be nested within randomly distributed ripples with sizes between 5 to 20 nm (Figure 1a and f) that are strongly reminiscent of the irregular ripples observed in suspended and supported graphene.[6−8] Similarly, the 3.6 Å buckling structure was nested within another 1D periodic ripple with a wavelength of 2−3 nm and with the same buckling direction (Figures 2 and 3e). However, the 1D nanoscale periodic ripple structure has relatively weak periodicity (with the wavelength varying slightly at different places), resembling the trench-induced mesoscopic ripples in graphene.[16] Strong evidence for the nesting of the 3.6 Å buckling structure into nanoscale periodic ripples is that the original diffraction peaks of the graphene lattice in the Fourier spectrum are broadened into lines strictly along the buckling direction (Figures 2 and 3c); this indicates that the angstrom-scale structures are embedded within a one-dimensionally curved 3D manifold. Although cascaded buckling has been observed in deformed plastic sheets,[28] it is unexpected in 2D crystalline sheets like graphene. Taken together, our findings suggest that the angstrom-scale buckling and the mesoscopic rippling are manifestations of distinct mechanical properties of graphene that may coexist in a linearly combined fashion.

To understand the potential changes in the physical properties of graphene arising from the angstrom-scale periodic buckling, we used DFT to calculate the electronic structures of the buckled graphene monolayers (see Supporting Information and Methods). The low-energy charge carriers in pristine graphene are well described by a massless Dirac equation and have a linear energy dispersion isotropic near the Dirac points (*K*) at the corners of the Brillouin zone (Figure 4a).[2] A previous theoretical study clarified that an anisotropy in energy dispersion near the Dirac points is realizable

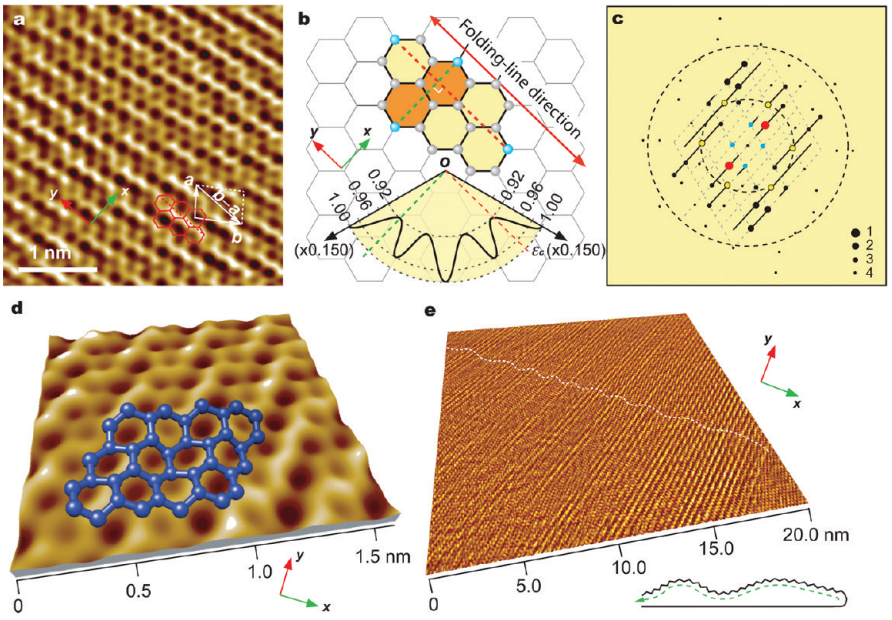

Figure 3. The 3.6 Å periodic buckling structure in a folded graphene monolayer. (a) Sub-angstrom resolution TEM imaging of the buckling structure in detail. The unit manifold is marked by red hexagons. Arrows a and b dictate the lattice vectors of the periodic buckling structure, where b−a is parallel to the *y*-direction. (b) The intrinsic geometric rule in the unit buckling manifold (upper panel) and the calculated angular distribution of the nominal critical strain (ε_c) at a distance of two unit cells (lower panel, drawn in polar coordinate system) that guides the buckling orientation and wavelength selection. The green dashed line parallels the buckling direction (*x*-direction). The red dashed line parallels the folding line (*y*-direction). Only $2\pi/3$ angular range is shown for the angular distribution of ε_c due to its 6-fold symmetry. (c) The merged Fourier spectrum of the 3.6 Å buckling structure. The IQ, from 1 to 4, is shown as the spot size. The red spots indicate the major buckling periodicity at 3.6 Å. The blue spots indicate the 2D lattice of the unit buckling manifold, corresponding to the lattice vectors a and b shown in panel (a). The yellow spots indicate the major diffractions arising from the original graphene lattice. (d) The 3D reconstruction of the topographic view of the buckling structure. The DFT-calculated 3D atomic configuration of the buckling structure with the lowest deformation energy (0.77 eV/atom) at the observed strain (0.15 in the *x*-direction and 0.04 in the *y*-direction), shown as a blue ball−stick model, was fitted into the 3D map. The buckling amplitude is greater in the *x*-direction (~0.9 Å) than in the *y*-direction (~0.3 Å). (e) The 3D perspective view of the buckling structure shows that the 3.6 Å buckling structure is nested within another set of 1D ripples of 2−3 nm wavelength with the same propagation direction. The white dashed line highlights the nanoscale ripples. There is more contrast and a slightly larger wavelength of the 3.6 Å buckling structure at the ripple top, as schematically modeled in the inset. In all panels, the green arrows indicate the major buckling orientation, and the red arrows indicate the folding-line direction.

in graphene under externally applied periodic potentials, owing to the chiral nature of charge carriers.[5] Our *ab initio* results suggest that the chirality may also give rise to a significant anisotropy in the energy dispersion of charge carriers in the angstrom-scale buckled graphene monolayers in the absence of external periodic potentials (Figure 4b−f). The Dirac cone in pristine graphene is circular and centered at the Dirac point (Figure 4a and d). By contrast, in the buckled graphene, the Dirac cone is significantly broadened and becomes oval; its horizontal cross-section is no longer centered at the Dirac point (Figure 4b−f). Such strong symmetry breakage implies a highly anisotropic propagation of charge carriers through graphene with the angstrom-scale buckling structures.[5] Other changes in graphene's properties induced by the angstrom-scale buckling are thus expected and deserving of systematic study.

The formation of the angstrom-scale buckling structures is expected to arise from the interlayer interactions in a bilayer or a folded monolayer with the assistance of liquid-phase processing (see Supporting Information, notes S3−S5 for details). The potential utilization of these fine buckling structures might ultimately allow miniaturization of strain-engineered graphene devices to several angstroms.[13−15] The anisotropic behaviors of massless Dirac fermions in the angstrom-scale buckling structures may endow graphene electronic circuits and devices with novel functions and utilities.[5] The substrate-free production of the periodic buckling structures also allows great flexibility in adapting them for diverse potential applications.

METHODS

Sample Preparation. Graphite flakes with a size of 1.8−5 mm (NGS Naturgraphit GmbH, Leinburg, Germany) were incubated in 1 mL *N*-methyl-pyrrolidinone (NMP, HPLC level, > 99%, Sigma-Adlrich) in a 1.5 ml glass vial and sonicated for 3 h in an ultrasonication bath (Input 160 W, output 70 W; Branson 1510, CT). The sonicated solution was then centrifuged at 500 rpm for 90 min. The upper suspension was decanted off the vial

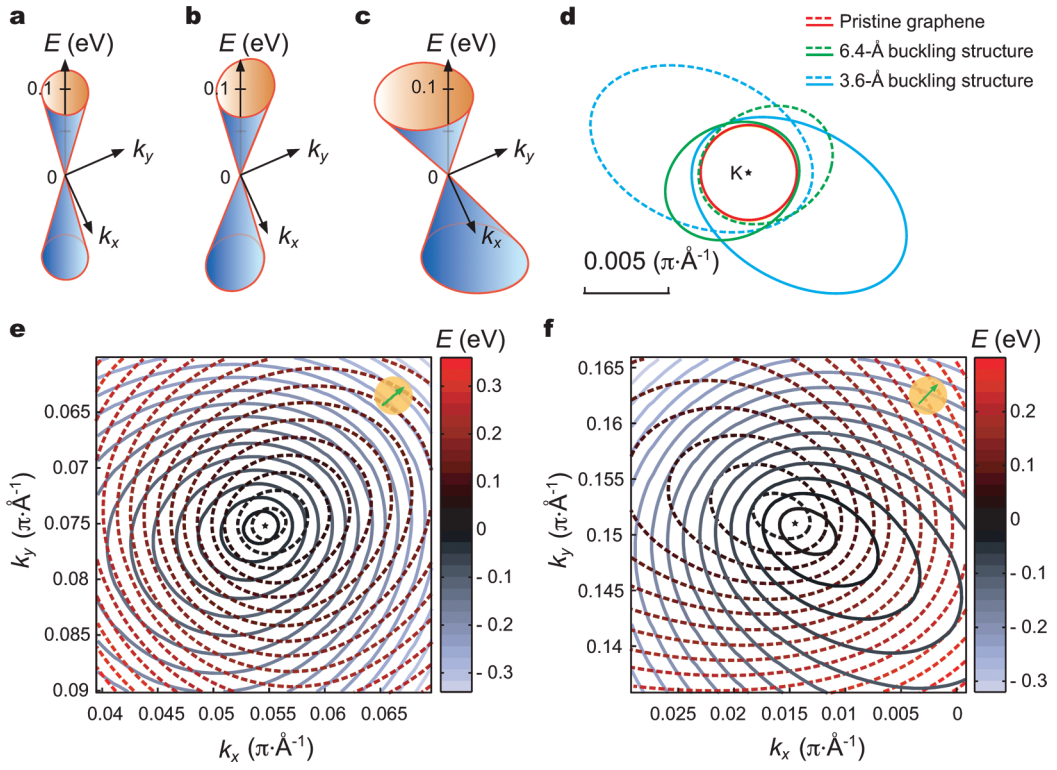

Figure 4. Anisotropic changes in the electronic structure of graphene induced by angstrom-scale buckling. (a) The isotropic energy dispersion near one of the Dirac points of charge carriers in pristine graphene. (b and c) The anisotropic energy dispersion near the Dirac points of charge carriers in graphene with the 6.4 and 3.6 Å buckling structures, respectively. The 3D plots in (a−c) are shown on the same scale. (d) Comparison of the energy dispersion at the same contour level ($E = 0.05$ eV as dashed lines, and $E = -0.05$ eV as solid lines) of pristine and buckled graphene, showing significant anisotropic changes induced by the angstrom-scale buckling. The Dirac points for the different structures are shifted and aligned to the same position in the k plane for comparison, as indicated by a black asterisk. (e and f) The contour plots of the energy dispersion around the Dirac points of charge carriers in graphene with the 6.4 and 3.6 Å buckling structures, respectively. The contours above the Dirac points are shown as dashed lines and the contours below the Dirac points by solid lines. The position of Dirac point at the center of each contour plot is marked by asterisk. The green arrows in (e and f) indicate the major buckling directions and correspond to the green arrows shown in Figures 1 and 3, respectively.

and was transferred to another clean vial for storage before use. The precipitated graphite flakes may be used again by exfoliation in another volume of the solvent. A 3 μL droplet of the graphene dispersion was applied to a holey carbon grid (C-Flat, 400 mesh size, 1.2/1.3R, Protochips, NC) and blotted by filter paper from the edge and backside of the grid. (A second droplet of the graphene dispersion may be applied to the same grid, which enhances the chance of observing the buckling structures.) The grid was then vacuum dried for 30−60 min before loading into the electron microscope specimen chamber.

TEM Analysis. The monochromated, aberration-corrected TEM (Libra 200MC, Carl Zeiss NTS, MA) equipped with a field-emission gun (80−200 kV) and an in-column omega energy filter was first aligned and adjusted with respect to the objective lens aberration corrector at 80 kV, with the monochromator and energy filter off, using an amorphous carbon film area, through the CETCOR software interface (CEOS GmbH, Heidelberg, Germany). After the objective lens spherical aberration was corrected up to the third order, the monochromator was switched in (4 μm slit). TEM imaging and analysis then were performed at near-Gaussian focus at room temperature and recorded by a 4000 × 4000 CCD camera (Gatan, Ultrascan4000, USA) at a nominal magnification of 1 000 000×. All image data reported in this paper were based on the same aberration correction parameters. Because of the integration of Z-axis density, transmission electron mirographs do not directly measure the sample height. Nonetheless, the height of rippling in 2D materials can still be estimated by either the Z contrast change of the atom volume or the geometric constraint of the atomic crystal order. In this work, we employed the latter approach, taking advantage of the rich information in atomic positions in the x−y plane and verified the results by DFT. Using the crystallographically analyzed geometric configuration of the unit buckling structure as shown in Figures 1c and 3b and assuming the average carbon−carbon bond length to be 1.42 Å, one can readily estimate the rippling height. The estimation gave 0.9 ± 0.3 Å for the 6.4 Å buckling structure, in agreement with the DFT result 1.2 Å, and 1.1 ± 0.3 and 0.5 ± 0.3 Å in the x- and y-directions, respectively, for the 3.6 Å buckling structure, agreeing with the DFT results of 0.9 (x) and 0.3 Å (y).

Theoretical Analysis and First-Principles Calculations. To calculate the critical strain ε_c as a function of chiral direction, we used a quantitative relationship (eq 1 in Supporting Information) that was yielded by a molecular mechanics simulation of graphene elasticity without imposing the approximation of continuum mechanics.[24] The calculation details are provided in Supporting Information, note S2 and Figure S3. The first-principles calculations were performed with the software package Spanish Initiative for Electronic Simulations with Thousands of Atoms (SIESTA) that implements the DFT.[30] The atomic structures, deformation energy, and band structures were calculated using localized atomic orbitals with an energy cutoff of 70 Ry (~952 eV). To calculate the atomic structures of the angstrom-scale buckling, the supercells containing 9 and 6 graphene unit cells (Figures 1c and 3b) were used for the 6.4 and 3.6 Å buckling structures, respectively. The structures were relaxed under given strains and periodic boundary conditions. The energy optimization was terminated when the magnitude of the force on each atom was less than 0.04 eV Å^{-1}. For the calculation of the 3.6 Å buckling structure, an extra geometric constraint exerted by the folding edge was taken into account; that is, in the supercell, 7 carbon atoms located around a line parallel

to the folding edge were limited in the extent of their out-of-plane displacement to ≤0.3 Å. No extra geometric constraint was used for the calculation of the 6.4 Å buckling structure. In all calculations, the Perdew−Burke−Ernzerhof exchange−correlation functional and a *k*-point mesh cutoff of 20 Å were used. As the *ab initio* atomic models of the buckling structures closely match the 3D reconstructions of the buckling structures generated by the *Z* contrast images of aberration-corrected TEM, the 3D coordinates of the *ab initio* atomic structures were used to extract the amplitudes of the buckling structures and were used as input parameters for the *ab initio* calculations of their corresponding energy dispersion. Although the *ab initio* calculations produced detailed atomic configurations that can directly explain the TEM observations, they alone cannot account for the selection of the angstrom-scale buckling wavelength. Instead, a semi-quantitative analysis is described in Supporting Information, note S4, that accounts for the selection of angstrom-scale wavelength, by combining results from the *ab initio* calculations and the dynamic theory of Euler buckling instability.

Acknowledgment. The authors thank D. C. Bell for assis tance and coordination in TEM imaging and maintenance and M. Lemme and Q. Ouyang for insightful discussion and comments. This work was supported by the National Institute of Health (NIH) (AI67854) and the Ragon Institute of MGH, MIT, and Harvard. The experiment was performed in part at the Center for Nanoscale Systems (CNS), a member of National Nanotechnology Infrastructure Network (NNIN), which is supported by the National Science Foundation under NSF award no. ECS-0335765. C.N.S. is part of the Faculty of Arts and Sciences at Harvard University.

Supporting Information Available: Details on TEM analysis and theoretical analysis, exclusion of the possibility that the TEM images of the buckling structures result from moiré fringe patterns, calculation of the critical strain as a function of chiral direction, a possible mechanism for the formation of the angstrom-scale periodic buckling, the selection of an angstrom-scale buckling wavelength, and symmetry breaking and reduced dimensionality of buckling. This material is available free of charge *via* the Internet at http://pubs.acs.org.

REFERENCES AND NOTES

1. Novoselov, K. S.; Geim, A. K.; Morozov, S. V.; Jiang, D.; Zhang, Y.; Dubonos, S. V.; Grigorieva, I. V.; Firsov, A. A. Electric Field Effect in Atomically Thin Carbon Films. *Science* **2004,** *306*, 666–669.
2. Novoselov, K. S.; Geim, A. K.; Morozov, S. V.; Jiang, D.; Katsnelson, M. I.; Grigorieva, I. V.; Dubonos, S. V.; Firsov, A. A. Two-Dimensional Gas of Massless Dirac Fermions in Graphene. *Nature* **2005,** *438*, 197–200.
3. Oostinga, J. B.; Heersche, H. B.; Liu, X.; Morpurgo, A. F; Vandersypen, L. M. K. Gate-Induced Insulating State in Bilayer Graphene Devices. *Nat. Mater.* **2008,** *7*, 151–157.
4. Zhang, Y.; Tang, T. T.; Girit, C.; Hao, Z.; Martin, M. C.; Zettl, A.; Crommie, M. F.; Shen, Y. R.; Wang, F. Direct Observation of a Widely Tunable Bandgap in Bilayer Graphene. *Nature* **2009,** *459*, 820–823.
5. Park, C. H.; Yang, L.; Son, Y. W.; Cohen, M. L.; Louie, S. G. Anisotropic Behaviours of Massless Dirac Fermions in Graphene under Periodic Potentials. *Nat. Phys.* **2008,** *4*, 213–217.
6. Meyer, J. C.; Geim, A. K.; Katsnelson, M. I.; Novoselov, K. S.; Booth, T. J.; Roth., S. The Structure of Suspended Graphene Sheets. *Nature* **2007,** *446*, 60–63.
7. Fasoline, A.; Los, J. H.; Katsnelson, M. I. Intrinsic Ripples in Graphene. *Nat. Mater.* **2007,** *6*, 858–861.
8. Geringer, V.; Liebmann, M.; Echtermeyer, T; Runte, S.; Schmidt, M.; Ruckamap, R.; Lemme, M. C.; Morgenstern, M. Intrinsic and Extrinsic Corrugation of Monolayer Graphene Deposited on SiO_2. *Phys. Rev. Lett.* **2009,** *102*, 076102.
9. Morozov, S. V.; Novoselov, K. S.; Katsnelson, M. I.; Schedin, F.; Ponomarenko, L. A.; Jiang, D.; Geim, A. K. Strong Suppression of Weak Localization in Graphene. *Phys. Rev. Lett.* **2006,** *97*, 016801.
10. Herbut, I. F.; Juricic, V.; Vafek, O. Coulomb Interaction, Ripples, and the Minimal Conductivity of Graphene. *Phys. Rev. Lett.* **2008,** *100*, 046403.
11. Elias, D. C.; Nair, R. R.; Mohiuddin, T. M. G.; Morozov, S. V.; Blake, P.; Halsall, M. P.; Ferrari, A. C.; Boukhvalov, D. W.; Katsnelson, M. I.; Geim, A. K.; et al. Control of Graphene's Properties by Reversible Hydrogenation: Evidence for Graphene. *Science* **2009,** *323*, 610–613.
12. Boukhvalov, D. W.; Katsnelson, M. I. Tuning the Gap in Bilayer Graphene using Chemical Functionalization: Density Functional Calculations. *Phys. Rev. B* **2008,** *78*, 085413.
13. Pereira, V. M.; Castro Neto, A. H. Strain Engineering of Graphene's Electronic Structure. *Phys. Rev. Lett.* **2009,** *103*, 046801.
14. Guinea, F.; Horovitz, B.; Le Doussal, P. Gauge Field Induced by Ripples in Graphene. *Phys. Rev. B: Condens. Matter Mater. Phys.* **2008,** *77*, 205421.
15. Guinea, F.; Katsnelson, M. I.; Geim, A. K. Energy Gaps and a Zero-Field Quantum Hall Effect in Graphene by Strain Engineering. *Nat. Phys.* **2010,** *6*, 30–33.
16. Bao, W.; Miao, F.; Chen, Z.; Zhang, H.; Jang, W.; Dames, C.; Lau, C. N. Controlled Ripple Texturing of Suspended Graphene and Ultrathin Graphite Membranes. *Nat. Nanotechnol.* **2009,** *4*, 562–566.
17. Vazquez de Parga, A. L.; Calleja, F.; Borca, B.; Passeggi, M. C. G., Jr.; Hinarejos, J. J.; Guinea, F.; Miranda, R. Periodically Rippled Graphene: Growth and Spatially Resolved Electronic Structure. *Phys. Rev. Lett.* **2008,** *100*, 056807.
18. N'Diaye, A. T.; Bleikamp, S.; Feibelman, P. J.; Michely, T. Two-Dimensional Ir Cluster Lattice on a Graphene Moiré on Ir(111). *Phys. Rev. Lett.* **2006,** *97*, 215501.
19. Sutter, P.; Sadowski, J. T.; Sutter, E. Graphene on Pt(111): Growth and Substrate Interaction. *Phys. Rev. B: Condens. Matter Mater. Phys.* **2009,** *80*, 245411.
20. Hernandez, Y.; Nicolosi, V.; Lotya, M.; Blighe, F. M.; Sun, Z.; De, S.; Mcgovern, I. T.; Holland, B.; Byrne, M.; Gun'ko, Y. K.; et al. High-Yield Production of Graphene by Liquid-Phase Exfoliation of Graphite. *Nat. Nanotechnol.* **2008,** *3*, 563–568.
21. Li, X.; Zhang, G.; Bai, X.; Sun, X.; Wang, X.; Wang, E.; Dai, H. Highly Conducting Graphene Sheets and Langmuir-Blodgett Films. *Nat. Nanotechnol.* **2008,** *3*, 538–542.
22. Batson, P. E.; Dellby, N.; Krivanek, O. L. Sub-Ångstrom Resolution Using Aberration Corrected electron optics. *Nature* **2002,** *418*, 617–620.
23. Golubovic, L.; Moldovan, D.; Peredera, A. Dynamics of the Euler Buckling Instability. *Phys. Rev. Lett.* **1998,** *81*, 3387–3390.
24. Lu, Q.; Huang, R. Nonlinear Mechanics of Single-Atomic-Layer Graphene Sheets. *Int. J. Appl. Mech.* **2009,** *1*, 443–467.
25. Lu, Q.; Arroyo, M.; Huang, R. Elastic Bending Modulus of Monolayer Graphene. *J. Phys. D: Appl. Phys.* **2009,** *42*, 102002.
26. Cadelano, E.; Palla, P. L.; Giordano, S.; Colombo, L. Nonlinear Elasticity of Monolayer Graphene. *Phys. Rev. Lett.* **2009,** *102*, 235502.
27. Lee, C.; Wei, X.; Kysar, J. W.; Hone, J. Measurement of the Elastic Properties and Intrinsic Strength of Monolayer Graphene. *Science* **2008,** *321*, 385–388.
28. Sharon, E.; Roman, B.; Marder, M.; Shin, G. S.; Swinney, H. L. Buckling Cascades in Free Sheets. *Nature* **2002,** *419*, 579.
29. Glaeser, R. M.; Downing, K.; DeRosier, D.; Chiu, W.; Frank, J. *Electron Crystallography of Biological Macromolecules*; Oxford University Press: New York, 2007.
30. Soler, J. M.; Artacho, E.; Gale, J. D.; Garcia, A.; Junquera, J.; Ordejon, P.; Sanchez-Portal, D. The SIESTA Method for *ab initio* Order-N Materials Simulation. *J. Phys.: Condens. Matter* **2002,** *14*, 2745–2779.